

Physical Context Detection using Wearable Wireless Sensor Networks

Muhannad Quwaider and Subir Biswas

Abstract: This paper presents the architecture of a wearable sensor network and a Hidden Markov Model (HMM) processing framework for stochastic identification of body postures and physical contexts. The key idea is to collect multi-modal sensor data from strategically placed wireless sensors over a human subject's body segments, and to process that using HMM in order to identify the subject's instantaneous physical context. The key contribution of the proposed multi-modal approach is a significant extension of traditional uni-modal accelerometry in which only the individual body segment movements, without their relative proximities and orientation modalities, is used for physical context identification. Through real-life experiments with body mounted sensors it is demonstrated that while the uni-modal accelerometry can be used for differentiating activity-intensive postures such as walking and running, they are not effective for identification and differentiation between low-activity postures such as sitting, standing, lying down, etc. In the proposed system, three sensor modalities namely acceleration, relative proximity and orientation are used for context identification through Hidden Markov Model (HMM) based stochastic processing. Controlled experiments using human subjects are carried out for evaluating the accuracy of the HMM-identified postures compared to a naïve threshold based mechanism over different human subjects.

Index terms: Body Area Network, Sensor Networks, Posture Identification, Context identification, Hidden Markov Model.

I. INTRODUCTION

Human health monitoring [1-5] is increasingly emerging as a dominant application framework for the evolving sensor network technology [6,7]. A number of tiny wireless sensors, strategically placed on a patient's body, can create a Wireless Body Area Network (WBAN) [8,9], that can monitor vital signs, providing real-time feedback to the patient, his or her doctors, and other medical service providers. Many patients diagnostics procures can benefit from such continuous monitoring of a chronic condition, or during recovery from an illness or surgical procedure. Recent technological advances in wireless networking promise a new generation of wireless sensor networks suitable for many of the health related applications as indicated above.

In this paper we deal with a body context identification problem in which a wireless network of body-mounted sensors is used for monitoring and identifying the instantaneous postures of a human subject. The spectrum of postures to be identified will include sitting, sitting-reclining, lying-down, standing, walking, jogging and other physical activities that relate to lifestyle and behavioral factors, and play a role in the etiology and prevention of many chronic diseases such as coronary heart disease and cancer. Once developed, such a wearable sensor network for posture identification can be used for patients' physical activity assessment for both surveillance and epidemiologic/clinical research purposes. Such automated instrumentation for physical activity and body posture detection has recently been actively promoted by various health oriented research organizations including the National Institute of Health (NIH) [10]. Additional applications of such body area sensing include real-time and remote monitoring of soldiers, elderly population, and athletes during workouts and sporting events.

In a number of projects [11-13] multi-axes accelerometers are used for identification of body postures by analyzing the level of accelerations in different body segments, which are a direct indication of physical activity. These mechanisms are shown to work [7,14,15] very well for identifying postures such as walking, jogging, and sprinting. However, for applications those require context identification at finer granularities, it is often necessary to differentiate between low-activity postures such as sitting, lying-down and standing; sometimes with even finer granularity such as sitting-upright or sitting-reclined. For these non activity-intensive postures, the traditional accelerometer based solutions do not work.

To address this limitation, in addition to the acceleration modality, we propose to add two new sensing modalities, namely, relative sensors proximity and sensor orientation. Relative proximity is measured using Received Signal Strength Indicator (RSSI) of the RF signal between two body-mounted sensor nodes. Information from multiple sensors is fused and stochastically processed using a Hidden Markov Model (HMM) for assessing the instantaneous body postures. The HMM is leveraged for dealing with sensing errors caused by a subject's clothing, body structure, irregular RF propagation, and the variability in sensor mounting.

This paper represents a generalized extension of our preliminary work [16] in which a conceptual wearable sensor network was developed for detecting only two body

Manuscript received in June 2008 and revised in September, 2008.

Authors are with Electrical and Engineering Department, Michigan State University, USA. e-mail: {quwaider, sbiswas}@egr.msu.edu

postures, namely, SIT and STAND. In this paper we extend those basic concepts to a generalized and more practical system that is capable of detecting a much wider set of postures including SIT, SIT-RECLINING, LYING-DOWN, STAND, WALK and RUN, by leveraging additional sensing modalities and a Hidden Markov Model (HMM) processing model. An online video demonstrating the preliminary working prototype can be found in [17].

II. WEARABLE SENSOR NETWORKS

A Wireless Body Area Network is constructed by mounting multiple sensor nodes in different segments of the body, as shown in Figure 1. Each sensor node can generate sensing data in all or a subset of all three target sensing modalities. As the wearable sensor nodes, Mica2Dot mote radio nodes, operating with a 900MHz radio, and its sensor card MTS510 from Crossbow Inc. [18] are used in our prototype system. The Mica2Dot nodes run from a 570mAH button cell with a total node weight of approximately 5.9 grams. In our experiments, each sensor is worn with an elastic band so that the sensor orientation does not change with respect to the body segments.

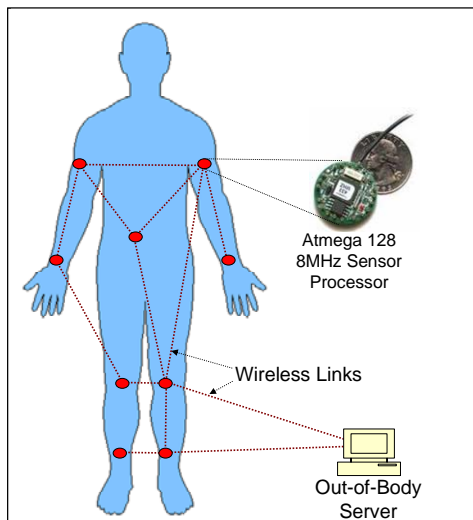


Fig. 1. Wearable wireless sensor network

As shown in the diagram, the wearable sensor nodes form an ad hoc sensor network with a topology that is dynamically determined based not only on the relative locations of a subject's body segments, but also on the quality of the wireless links. Wireless links are also available to transport raw data or processed events from the body network to an external processing server. A Mica2Dot radio node with custom-built serial interface, running RS232 protocol, has been used for collecting data from the body network and for sending to a Windows PC processing server.

A. Target Sensor Modalities

Three sensor modalities, namely, acceleration, relative proximity and orientation are used. A two-axes [12] piezoelectric accelerometer in the Mica2Dot sensor card is used for detecting the body movements. Acceleration data is generated in the units of gravitational acceleration g . While a near-zero acceleration may mean a very low activity posture such as sitting or lying-down, a high acceleration can indicate a high activity posture such as jogging or running.

The proximity between the sensor nodes is the second sensor modality that is measured in dB using received signal strength indication (RSSI) of radio frequency (RF) signal. Each sensor is set to periodically send a *Hello* message with a preset transmission power that is enough to reach all sensors on the body. Based on those *Hello* packets, each node creates and maintains a neighbor table, with information regarding RSSI for all other sensor nodes on the body. This way each node maintains a measure of the relative proximity with respect to the other nodes. Low RSSI values (high signal strength) indicate that the body parts are positioned relatively *close* to each other like during a sitting posture. Similarly, relatively higher RSSI values indicate that the corresponding body parts are relatively farther apart (e.g. during standing posture).

Sensor orientation is the third modality that can indicate the orientation of a body segment to which a specific sensor node is attached to. Orientation information can be used for identifying low activity orientation specific postures such as lying down and reclining. The two-axes [11] piezoelectric accelerometer in Mica2Dot sensor card is also used for orientation detection. The constant component of accelerometer's output indicates a sensor node's orientation. Orientation output is extracted by integrating the acceleration output, and can be assessed for both X and Y directions by the corresponding accelerometer outputs. Therefore, the orientation indicator shares the same unit as that for the raw accelerometer output.

B. Computation Modes

As shown in Table I, body context identification can be categorized into four computation modes: out-of-body offline, on-body offline, out-of-body online, and on-body online. For the out-of-body case, all sensor data is wirelessly collected to an out-of-body processing server (see Figure 1) which is used for the context identification. In on-body scenarios, the identification processing is performed at the sensor nodes themselves, either at a single node or at multiple nodes for improved processing load distribution. The offline and online processing modes represents whether the identification is done in real-time or not. For online processing, the amount of available sensor data is generally less than what is available in the offline scenarios.

TABLE I
COMPUTATION MODES AND THEIR APPLICATIONS

	Offline	Online
Out-of-body	Indoor workout, fitness evaluation	Indoor patient and elderly monitoring
On-body	Outdoor workout, fitness evaluation	Outdoor patients, soldiers and sports monitoring

From an application standpoint, the on-body processing is more suitable for the outdoor applications since a separate processing server may not be usually available. In indoor settings, however, such servers may be available and therefore the out-of-body applications can be supported. As summarized in Table I, real-time monitoring applications, out-of-body or on-body, is better supported using the online processing mode. Applications that require post-collection evaluation are better suited for the offline mode. Results presented in this paper correspond to out-of-body and offline computation mode. The prototype system described in this paper performs out-of-body and offline posture identification.

III. UNI-MODAL ACCELEROMETRY

This section outlines the identification process using a traditional uni-modal approach [11-13] using only the acceleration information. Controlled experiments are designed in which human subjects are given pre-determined sequences of postures (from the set SIT, STD, REC, DWN, WLK, and RUN) to follow, and a three-node wearable sensor network is used for collecting acceleration data from *right thigh, upper right arm, and right ankle*. Postures, identified using context detection algorithms, are then temporally correlated with the actual sequence given to the subjects for evaluating the identification accuracy.

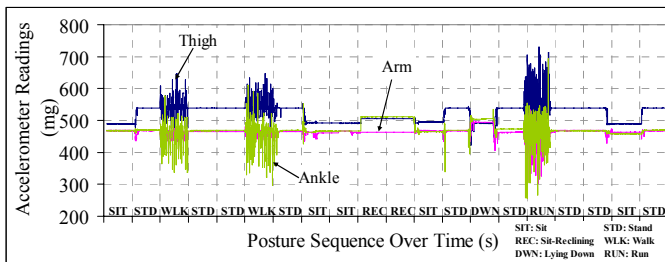


Fig. 2. Accelerometer data during a controlled posture sequence

Figure 2 shows the accelerometers readings in milli-g (1 mg is 9.81 mm/s^2) from all three sensor nodes, while a human subject was following a controlled 20-postures sequence as shown along the horizontal axis of the figure. Each posture slot in this experiment had lasted for approximately 20 seconds. A sampling rate of 20 Hz has been used for obtaining reading from the accelerometers. The numbers in the figure correspond to the average of the acceleration recorded in both the axes of the used sensor.

The figure shows as to how the accelerations readings

increase for the activity-intensive postures such as WLK and RUN compared to low-activity postures such as SIT and STAND. In fact the readings for SIT, REC, DWN and STD are almost the same due to the absence of any major physical activity in these postures.

The frequency domain representation of the collected accelerometer data is presented in Figure 3 for all six postures individually. The graph for WLK, for example, is plotted by applying Fourier Transform to the cumulative acceleration data from all the WLK states as shown in Figure 2. The same applies to the other postures as well.

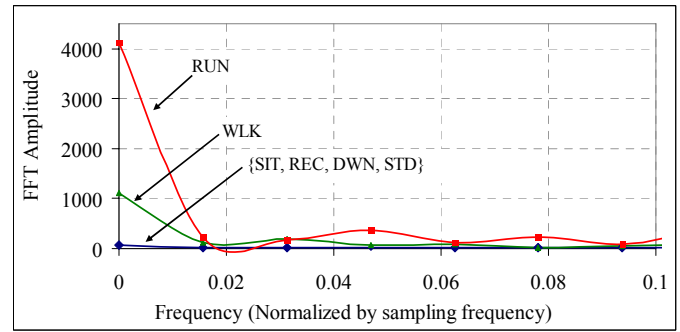


Fig. 3. Frequency domain view of the acceleration reading

Observe that while the graphs for WLK and RUN demonstrate a noticeable presence of frequency components in the range 0 to 0.1, the ones for SIT, REC, DWN and STD are almost flat over the entire frequency spectrum. The difference in the peak values for WLK and RUN indicate the difference of activity levels in those two postures. These peak values, coupled with suitably chosen thresholds, can be used for identification and differentiation between the WLK and RUN postures. The results in Figures 2 and 3 confirm that while uni-modal accelerometry is capable of identifying WLK and RUN, it is not sufficient for the low activity postures.

IV. MULTI-MODAL SENSING

In addition to accelerometry, additional sensing modalities, namely, relative proximity and orientation of body segments can be used for differentiating among the low-activity postures such as SIT, REC, DWN and STD. In this section we provide experimental details for identifying all six target postures using three sensor nodes operating in three sensors modalities.

A. Sensor Placement and Modality Usage

Three sensor nodes are mounted at three body locations, namely, the right thigh, the upper right arm and the right ankle. The thigh sensor is used for capturing body acceleration, while all three sensors are used for detecting the relative proximities between all sensor pairs, and both arm and ankle sensors are used for sensing the orientations of those body parts. Through extensive experimentation with different subject individuals it was found that the above sensor placement can provide enough information diversity

for all three sensing modalities for them to be applicable to our proposed posture identification process.

A summary of placement, supported modality, and target posture information is shown in Table II. While all three nodes are programmed to provide RSSI based proximity data, the nodes on the arm and ankle are used for generating orientation information, and the sensor node on thigh is used for assessing a subject's level of bodily acceleration. The last column indicates as to the identification of which set of physical postures that each specific sensor node contributes towards. Throughout the rest of the paper the target postures will be abbreviated as: SIT (sit straight), STD (stand), REC (sit reclining), DWN (lying down), WLK (walk), and RUN (run).

TABLE II
ON-BODY SENSOR MODALITY AND PLACEMENT SUMMARY

Sensor Node ID	Sensor Placement	Supported Modality	Target Postures
1	Upper Right Arm	Orientation, Proximity	SIT, DWN, STD
2	Lower Right Ankle	Orientation, Proximity	SIT, REC, DWN, STD
3	Right Thigh	Acceleration, Proximity	WLK, RUN, SIT, STD

Note that while more sensors provide richer set of data to work with, it also makes the overall sensor wearing process increasingly cumbersome. Therefore, a key objective of the system design is to achieve high posture identification success with as few sensor nodes as possible. Also, it was found that due to the variability of the RF links caused primarily by body movements, antenna mis-orientation, and signal blockage by clothing material, not only the network topology becomes unpredictably dynamic, but the proximity information indicated by the RSSI values can also vary over a very large range. This has the potential for introducing serious inaccuracies in the posture identification unless specific measures are taken to suppress the effects of such measurement errors. A Hidden Markov Model has been used to specifically address these measurement errors and variability.

B. Posture Modeling and Generation

The posture transitions of a human subject are modeled as a *Markov Process* in which the subject's posture transitions assume to follow a memory-less process [19]. The transition probabilities across the postures, as shown in Figure 4, represent a subject's behavior that is assumed to remain stationary for a certain time interval. The corresponding transition matrix, termed as A , remains fixed during such an interval, and can vary across the intervals when there is a broad change in behavior. In the following experiments we generate a sequence of 50 postures states using the transition

probability matrix:

$$A = [a_{i,j}] = \begin{bmatrix} 0.5 & 0.2 & 0.1 & 0.2 & 0 & 0 \\ 0.5 & 0.5 & 0 & 0 & 0 & 0 \\ 0.2 & 0 & 0.5 & 0.3 & 0 & 0 \\ 0.3 & 0 & 0.1 & 0.4 & 0.1 & 0.1 \\ 0.1 & 0 & 0.1 & 0.2 & 0.4 & 0.2 \\ 0 & 0 & 0.1 & 0.2 & 0.3 & 0.4 \end{bmatrix},$$

in which the states 1 through 6 represent the postures SIT, REC, DWN, STD, WLK and RUN respectively.

As a part of each experiment, a human subject is handed out the resulting posture sequence and is instructed to follow the sequence with 20 sec being spent in each posture, thus the entire experiment lasting for 1000 sec. Note that the transition matrix A is chosen based on long observation of typical behavioral pattern of multiple human subjects in our laboratory setting.

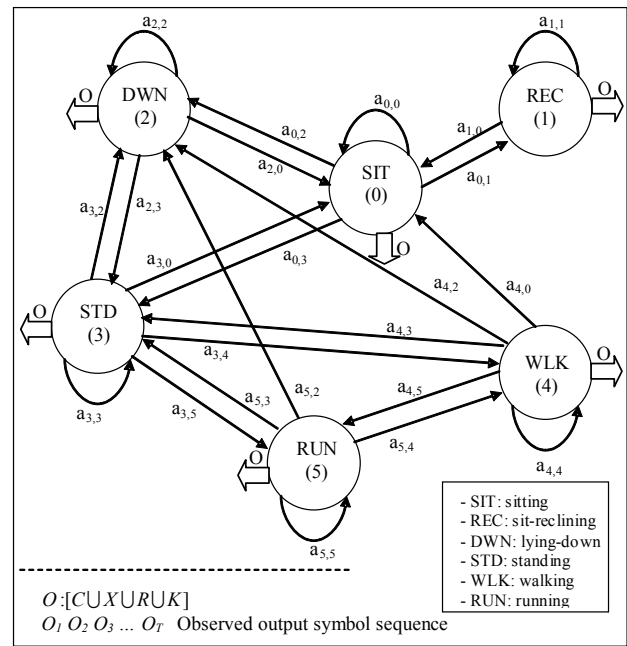


Fig. 4. Posture state transition machine

C. Threshold based Identification

The flowchart in Figure 5 depicts a mechanism in which context identification is accomplished by applying different thresholds for all three sensing modalities. After the low and high activity postures are separated using the degree of acceleration recorded by the node on the thigh, a proximity threshold (applied in terms of RSSI) is used to distinguish between STD (stand) and the other remaining postures, namely, SIT, REC, and DWN. The lying-down (DWN) posture can subsequently be separated using the orientation information from the node on the arm. Finally, the differentiation between SIT and REC is performed based on the orientation information from the ankle. Details about the exact threshold values used for different sensor modalities are presented in Table III. Results presented in this section

correspond to an out-of-body and offline computation mode.

TABLE III
Threshold group values for context identification

Threshold Group	Moderate Activity Level (mg/s)	High Activity Level (mg/s)	Avg. RSSI (dB)	Arm Ornt. (mg)	Ankle Ornt. (mg)
Thr_1	5	20	80	460	470
Thr_2	5	30	70	470	480
Thr_3	8	30	80	480	490
Thr_4	8	30	90	490	500
Thr_5	8	30	100	500	510
Thr_6	8	30	110	510	520
Thr_7	8	30	120	520	530
Thr_8	8	30	130	530	540

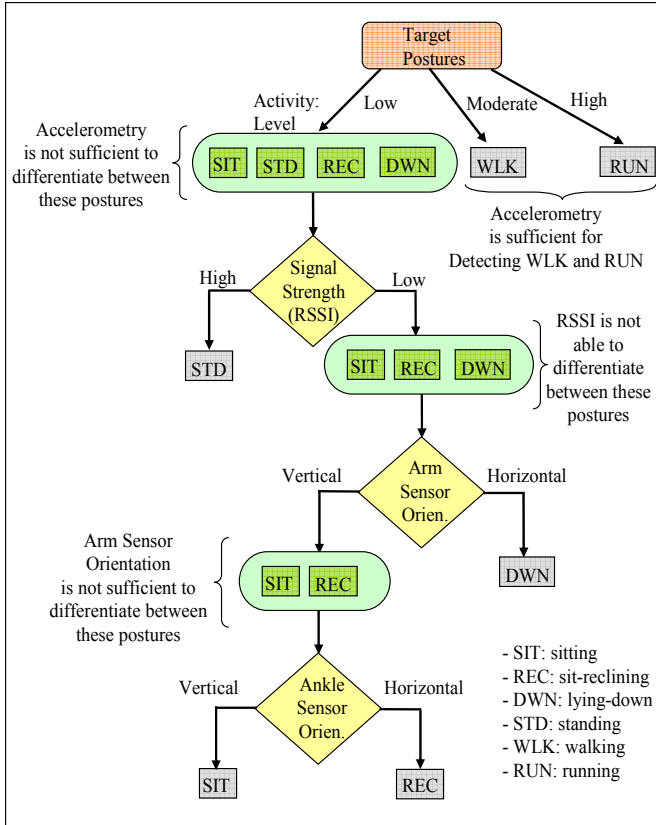


Fig. 5. Posture identification using multi-modal thresholds

Sensor reading for all three modalities and the corresponding actual postures for all 50 posture slots are reported in Figure 6. For the sake of brevity, the postures SIT, REC, DWN, STD, WLK and RUN are identified by the letters S, R, D, T, W and U respectively. The actual state (the posture that the subject is in) during a slot is reported by the corresponding letter on the horizontal axis during the slot. With each slot lasting for 20 seconds, the entire experiment corresponds to 1000 seconds, representing 50 posture slots.

The graph in Figure 6:a reports the actual posture states and the corresponding activity levels, which are computed as the absolute value of the first order derivative of the raw accelerometer output. The derivative represents the difference between two successive acceleration samples collected at 20 Hz sampling rate. The computed derivative numbers are then integrated using a moving average with window size of 5 sampling slots. Finally, those integrated derivative numbers for both X and Y directions (using the accelerometer outputs for both X and Y axes from the thigh-mounted sensor) are averaged to produce the activity levels that are plotted in Figure 6:a. As expected, the activity levels are high for the W and U (WALK or RUN) slots, and low for all other posture slots.

Average proximity information from all three sensor nodes, along with the actual postures, is reported in Figure 6:b. Each node periodically (once in every *Hello* interval of 1.5 seconds) computes the average RSSI value based on the radio signal reception through *Hello* packets from the other two nodes, and then wirelessly send that data to the thigh-mounted sensor. This thigh sensor then computes a master average based on the averages received from the other two sensors and its own average. This final average (in dB), which is reported in Figure 6:b, is then wirelessly transmitted to an out-of-body machine for further processing. In these readings, high RSSI dB values indicate low received radio signal strength and vice versa.

The following observations should be made from Figure 6:b. First, the average RSSI has an overall trend to be the lowest for SIT (S) and the highest for STAND (T). This is consistent since the body parts are generally closely situated during sitting, and further apart while standing. The average RSSI values for the other two low-activity postures SIT-RECLINE (R) and LYING-DOWN (D) fall in between those for S and T. Second, while generally maintaining this trend, there are certain anomalies caused by several factors including radio signal blockage by the clothing material, unintentional change of sensor node and antenna orientations, and various other imperfections in sensor mounting.

Figures 6:c and 6:d show the X -direction orientation indication (as introduced in Section II.A) for the sensor nodes attached to the arm and the ankle respectively. Orientation indication is computed by first averaging the raw accelerometer output over 20 samples (i.e. 1 second), and then integrating those average values using a moving average with window size of 5. Both sensors on the arm and the ankle are mounted such that high X -direction orientation values in Figures 6:c and 6:d indicate horizontal orientations of the corresponding body segments, and low values represent relatively vertical orientations. Note that the Y -direction orientation information is not used in these experiments.

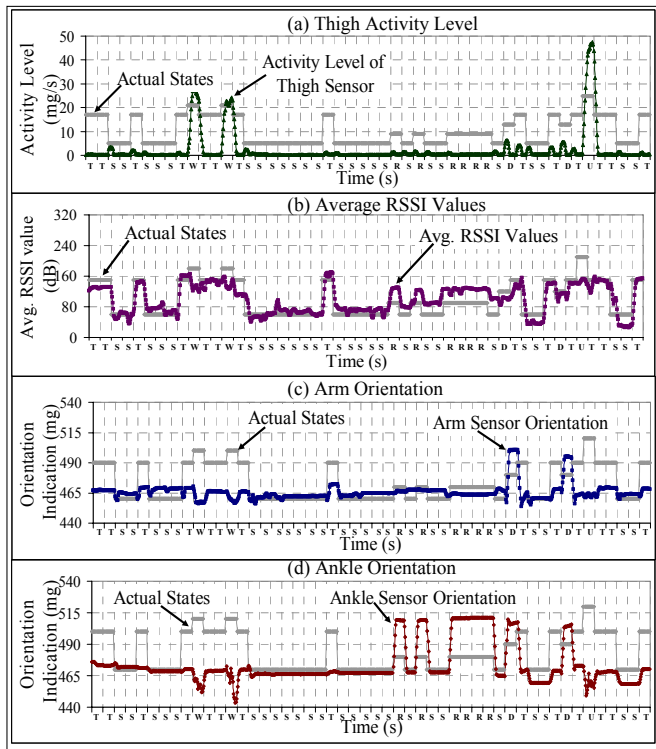


Fig. 6. Sensor outputs and actual postures

The arm sensor orientation in general can be used to detect the LYING-DOWN (D) posture, since it is evident in the plot that the arm sensor orientation readings in D postures are distinctively more horizontal (higher values) compared to those during other postures. Also, the ankle sensor orientation can be used to detect both LYING-DOWN (D) and SIT-RECLINING (R), because the orientations of the ankle in these two postures are also distinctively more horizontal (higher values) compared to the other two low-activity postures SIT (S) and STAND (T). Note that the sensor data patterns, as seen in Figure 6 for all modalities, are consistent with the threshold based context identification logic presented in Figure 5.

Threshold values of all sensor modalities at different sensors are depicted in Table III. Each set of threshold combinations are grouped together, and eight such groups are depicted in the table. The first and the second columns represent the moderate and the high activity level thresholds to be applied on readings from the thigh-mounted sensor node for differentiating between the WLK and RUN postures (see Figure 5). The third column represents RSSI threshold for the master average RSSI value collected and computed at the thigh sensor node. The last two columns indicate threshold values to be applied on the orientation readings from the arm and the ankle mounted sensor nodes respectively.

Figure 7 depicts the threshold based context detection accuracy computed over the 50-state posture sequence generated by the A matrix reported in Section IV.B. Using the thresholds specified in Table III, the comparison algorithm from Section IV.B has been applied to the multi-modal sensor data obtained from all three body-mounted sensors for identifying the instantaneous body posture. The identified

posture is then compared with the subject's actual posture for computing the success rate as reported in the Figure. Such success rates are presented as percentage matches for different threshold groups and for different human subjects. Three individuals in these experiments were asked to follow the same controlled posture sequence as used in Figure 6 for several rounds, before the identification performance were computed.

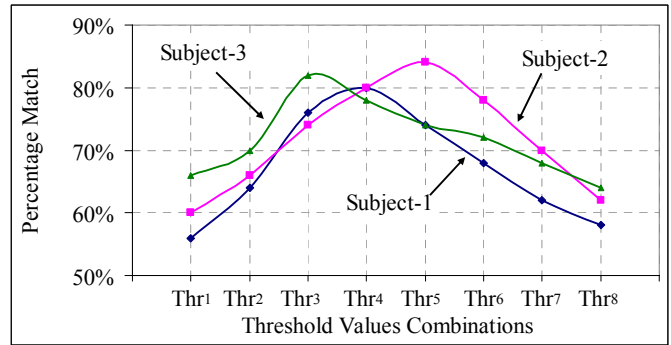


Fig. 7. Detection accuracy for multiple human subjects

Observe that in spite of the errors contributed by sensor and antenna mis-orientation and radio signal blockage by clothing material, this threshold based mechanism can detect the six postures with up to approximately 84% accuracy. However, since the identification success rate is heavily sensitive to the threshold values, choosing the right threshold values is an important design step for this mechanism to work.

A potentially restricting aspect of this threshold-based mechanism is that the optimal threshold values (threshold groups in this case) are also sensitive to the individual subjects' physical and motor aspects during his or her postures. For example, while the threshold group Thr_5 yields the best identification accuracy of 84% match rate for subject-2, the performance for subject-3 maximizes at 82%, for the threshold group Thr_3 . In fact, at Thr_5 , for subject-3 the system delivers a poor posture identification rate of only 74%. These results allude to a practical limitation of the threshold based posture identification in terms of the need for person specific threshold dimensioning. Other experiments further indicated that the optimal threshold value can change even for an individual based on his or her behavioral changes over time. In the next section we develop a Hidden Markov Model (HMM) based mechanism for adaptive and subject-independent posture detection.

V. CAPTURING STATIONARY BEHAVIOR USING HIDDEN MARKOV MODEL

The inability of the threshold based mechanism to handle the degraded quality of sensor data stems from the fact that the identification process does not leverage the stationary nature of human behavior over certain time intervals. To address this limitation, we adopt a stochastic posture identification solution that attempts to leverage the stationary

nature of human posture by modeling the posture state machine as a Hidden Markov Model (HMM) [20].

The key concept of the HMM [20] are as follows. A stochastic process is represented by a discrete time Markov Chain consisting of multiple states which are hidden from an observer in the sense that an observer cannot directly determine which state the system is in at any given point in time. However, a number of observable parameters, stochastically representing the states, are visible to the observer. The idea of HMM formulation is that if the state transition probability matrix and the observation generation probabilities are known (or measurable) to the observer, the latter can estimate the current state of the Markov Chain. Using HMM it is also possible to compute the probability of occurrence of a specific state sequence [21-24].

A. HMM Mapping

The posture identification problem with multi-modal sensing framework is mapped as an HMM formulation as follows.

Posture State Space: N postures are modeled as N hidden states with the state space represented by $S = \{S_1, S_2, \dots, S_N\}$. In this specific case $N = 6$, for postures SIT, SIT-RECLINING, LYING-DOWN, STAND, WALK and RUN.

Observation: At each state, the observation is represented by a vector O , which is constructed by combining four sub-vectors $O = [C \cup X \cup R \cup K]$, where C represents the activity level information from the thigh sensor, X represents the master average RSSI value from all three sensors, and R and K represent the orientation indications from the arm and ankle sensors respectively. HMM observation vectors are constructed from the multi-modal sensor data as shown in Figure 6. Each sub-vector is created as follows.

The activity level observation at any point in time is represented by the sub-vector $C = \{c_1, c_2, \dots, c_{MC}\}$, in which each c_m ($m = 1, 2, \dots, MC$) is a binary variable which can be either '0' or '1'. The peak-to-peak activity level range (see Figure 6:a) is divided into MC equal windows, and then depending on which window the current activity level falls in, the corresponding c_m is set to '1', and the rest of the sub-vector elements are set to '0'. Note that the value of MC determines the granularity of observation, which in turn, is expected to influence the quality of the hidden posture state identification process. The Window Boundary (WB) points for the sub-vector C is represented by WB_C . The number of WB points is one less than the value of MC .

Observation sub-vectors X , R , and K for RSSI values and orientation indications from the arm and the ankle sensors are constructed using the same mechanism as used above for the activity level sub-vector C . The corresponding granularity factors (e.g. the sub-vector size) are indicated as MX , MR and MK respectively, and the window boundary points are represented by WB_X , WB_R , and WB_K respectively.

At any time instant t , all four sub-vectors are combined into an overall observation vector O_t . Also, an overall observation granularity factor M is computed by adding the individual granularity factors MC , MX , MR and MK . The minimum value of M in our system was chosen to be 9, with

corresponding values of MC , MX , MR and MK to be 3, 2, 2, and 2 respectively. We have experimented with various values of M , ranging from 9 (coarse granularity observation) to 15 (fine granularity observation). For M to be 15, MC , MX , MR and MK were chosen to be 4, 5, 3, and 3 respectively.

Consider an example in which M is chosen to be 9 with MC , MX , MR and MK as 3, 2, 2, and 2, and the window boundaries WB_C , WB_X , WB_R , and WB_K are chosen as {8, 30} mg/s, 90 dB, 490 mg, and 500 mg respectively. Now with raw sensor outputs representing activity level of 4 mg/s, RSSI of 70 dB, and arm and ankle orientation indications of 470 mg and 480 mg, the resulting sub-vectors C , X , R , K will be [1,0,0], [1,0], [1,0], and [1,0] respectively. Therefore, the overall observation vector O will be [1, 0, 0, 1, 0, 1, 0, 1, 0].

As indicated in Figure 4, the parameter O_t represents the observation vector at time slot t , with T as the final observations in an experiment. In all our experiments, the value of T is 50. In other words, 50 observations, each corresponds a state lasting for 20 seconds, are generated to feed into the HMM estimation system.

Transition Probability Matrix: The posture transition probability matrix is represented as $A = [a_{ij}]$, where

$$a_{i,j} = p(q_t = S_j | q_{t-1} = S_i), \quad 1 \leq i, j \leq N \quad (1)$$

A is an $N \times N$ matrix, where N corresponds to the number of postures (states), which is 6 in our case. The quantity q_t denotes the actual posture at time t . The parameter $a_{i,j}$ represents the probability that the next posture is j , given the current posture of the subject is i .

Observation Probability Matrix: As done for the observation vector O , the observation probability matrix B is constructed by combining four sub-matrices as $B = [BC \cup BX \cup BR \cup BK]$, where BC , BX , BR and BK correspond to activity level, RSSI and orientation indications from the arm and the ankle sensors respectively.

The elements of sub-matrix BC , whose dimensions are $N \times MC$, are represented by:

$$b_{j,m} = p(C = [c_1 = 0, \dots, c_m = 1, \dots, c_{MC} = 0] | q_t = S_j), \quad 1 \leq j \leq N, 1 \leq m \leq MC, \quad (2)$$

where C represents the activity level observation sub-vector. The parameter $b_{j,m}$ represents the probability that in posture state j , the element c_m in the observation sub-vector C is '1' and the rest of the elements in C are all zeros. In other words, when a human-subject is in postures state j (j can be one of six targeted postures in our system), the quantity $b_{j,m}$ indicates the probability that the observed activity level falls in the m^{th} window of observation within the sub-vector C .

Following the same mechanism as used above for the activity level, observation probability sub-matrices BX , BR , and BK are constructed for observed RSSI and orientation indications from the arm and the ankle sensors. The dimensions of those sub-matrices are $N \times MX$, $N \times MK$, and $N \times MR$. Combining all four sub-matrices, as shown below, the overall observation probability matrix B with dimension $N \times$

M is constructed.

Initial State Distribution: This is represented by a vector $\pi = [\pi_i]$ of length N , so that:

$$\pi_i = p(q_0 = S_i), \quad 1 \leq i \leq N \quad (3)$$

The quantity π_i represents the probability that the posture Markov chain is initialized at state i . By definition, $\sum_{i=1}^N \pi_i = 1$.

Based on the above definitions, a system, modeled using HMM, can be fully specified by the parameters A , B and π which are represented together as a tuple:

$$\lambda = (A, B, \pi) \quad (4)$$

As presented in the next section, we first compute the individual probabilities of the system being in each possible posture state at a given time. As shown in the derivation, these probabilities depend on the system's λ , and the observation sequence $\{O_1 O_2 O_3 \dots O_T\}$. After the probabilities are computed, the posture state identification is accomplished by finding the most likely state, which is the one with the highest current probability.

B. Posture Detection using HMM

The probability of observing a given sequence $O = \{O_1, O_2, \dots, O_T\}$ of length T time steps is represented as $P(O|\lambda)$, and can be evaluated using the forward-backward procedure [22], as follows:

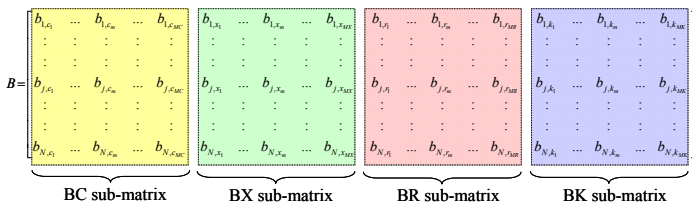
$$P(O|\lambda) = \sum_{i=1}^N \alpha_T(i), \quad (5)$$

where $\alpha_T(i)$ is referred to as forward variable, and defined as:

$$\alpha_t(i) \equiv P(O_1, O_2, \dots, O_t, q_t = S_i | \lambda), \quad 1 \leq i \leq N \quad (6)$$

It represents the probability that the partial sequence O_1, O_2, \dots, O_t , until time step t , has been observed and the current posture state at time t is S_i , given the HMM model λ . $\alpha_t(i)$ is a vector of dimension N (which is the total number of possible states). Another variable $\beta_t(i)$, referred to as backward variable, is defined as:

$$\beta_t(i) \equiv P(O_{t+1}, \dots, O_T | q_t = S_i, \lambda), \quad 1 \leq i \leq N \quad (7)$$



This represents the probability that the partial sequence from time step $(t+1)$ to the end has been observed and the current posture state at time t is S_i , given the model λ . $\beta_t(i)$ is also a vector of dimension N . Now another variable $\gamma_t(i)$ is defined such that:

$$\gamma_t(i) = p(q_t = S_i | O, \lambda), \quad (8)$$

where $\gamma_t(i)$ represents the probability of being in state S_i at time t , given an observation sequence O , and the model λ . Equation (8) can be expressed in terms of the forward-backward variables as:

$$\gamma_t(i) = \frac{\alpha_t(i) \beta_t(i)}{p(O|\lambda)} = \frac{\alpha_t(i) \beta_t(i)}{\sum_{i=1}^N \alpha_t(i) \beta_t(i)} \quad (9)$$

which is a vector of dimension N at time t . Using $\gamma_t(i)$ we can solve for the individually most likely posture state q_t at time t [20], as:

$$q_t = \arg \max_{1 \leq i \leq N} [\gamma_t(i)], \quad 1 \leq t \leq T \quad (10)$$

This q_t represents the detected posture state at time t .

C. Experimental Results

C.1 Manual Calibration

In this section we describe the performance of HMM based posture identification and its performance in comparison with the threshold based approach described in Section IV.C. The same transition probability matrix

$$A = [a_{i,j}] = \begin{bmatrix} 0.5 & 0.2 & 0.1 & 0.2 & 0 & 0 \\ 0.5 & 0.5 & 0 & 0 & 0 & 0 \\ 0.2 & 0 & 0.5 & 0.3 & 0 & 0 \\ 0.3 & 0 & 0.1 & 0.4 & 0.1 & 0.1 \\ 0.1 & 0 & 0.1 & 0.2 & 0.4 & 0.2 \\ 0 & 0 & 0.1 & 0.2 & 0.3 & 0.4 \end{bmatrix},$$

as used for the previous experiments, is used for generating a posture sequence to be followed by the human subjects. Note that for the results in this Section, the A matrix used for posture sequence generation is also used for the HMM model formulation. In other words, it is assumed that the A matrix used for HMM is already trained. During an initial set of known states, the B matrix is first computed, and then the actual posture identification process was initiated. This initial period is referred to as an *observation calibration* phase. As

for the Initial State Distribution matrix π , we have used $[0, 0, 0, 1, 0, 0]$, for all the experiments results presented here. This means that in all experiments the subject should start with the posture STAND. These A , B and π matrices constitute the HMM system parameter λ .

State identification using λ has been carried out using the HMM technique described in Section V.B. Figure 8 reports the posture identification performance with HMM in comparison with the threshold based mechanism as introduced in Section IV.C. As done before, the success rates are measured by comparing the identified postures with the actual postures from the generated posture sequence using transition probability matrix A .

The success rate for posture identification using HMM is reported with seven different observation granularities corresponding to $M = 9, 10, 11, 12, 13, 14$, and 15 . For each such values of M , the corresponding values of MC , MX , MR and MK , and their observation window boundaries are summarized in Table IV.

The first entry for $M = 9$ ($MC=3$, $MX=2$, $MR = 2$ and $MK = 2$) indicates that the three window levels for the C sub-vector are realized with two window boundaries WB_C of 8 mg/s and 30 mg/s. Similarly, two window levels for the X sub-vector are realized with one window boundary WB_X of 90 dB. Observe in the table that with increasing observation granularities (higher MC , MX , MR and MK) a larger number of window boundaries are needed to implement higher number of observation window levels.

TABLE IV
OBSERVATION SUB-VECTORS AND WINDOW BOUNDARIES FOR DIFFERENT OBSERVATION GRANULARITIES

M	MC, MX, MR, MK	WB_C	WB_X	WB_R	WB_K
9	3,2,2,2	{8,30}	90	490	500
10	3,3,2,2	{8,30}	{80,90}	490	500
11	3,4,2,2	{8,30}	{70,80,90}	490	500
12	3,5,2,2	{8,30}	{70,80,90,100}	490	500
13	3,5,3,2	{8,30}	{70,80,90,100}	(490, 500}	500
14	3,5,3,3	{8,30}	{70,80,90,100}	(490, 500}	(490, 500}
15	4,5,3,3	{8,30,40}	{70,80,90,100}	(490, 500}	(490, 500}

The following observations are to be made from Figure 8. First, the HMM approach delivers better state match rates (for example 84% to 96% identification success for human subject-2) compared to the best case performance using the threshold based mechanism (84% identification success for the same subject), that is with the threshold group 4 (8, 30, 70, 490, 510) as shown in Table III. Second, higher observation granularity (larger M) for HMM provides better posture identification success rate, with performance saturation occurring beyond the granularity factor around $M = 12$. Third, once a sufficiently large observation granularity (e.g. $M = 15$)

is chosen for HMM, unlike in the threshold based scheme, no optimal parameter dimensioning is needed. This is a significant advantage in terms of implementation feasibility. Finally, with similarly large observation granularities, the HMM continues to provide superior posture identification performance in a human subject-independent manner. This further reinforces the practicality of the mechanism in not having to dimension any individual-specific parameter which may cause significant performance variation as observed for the threshold based mechanism.

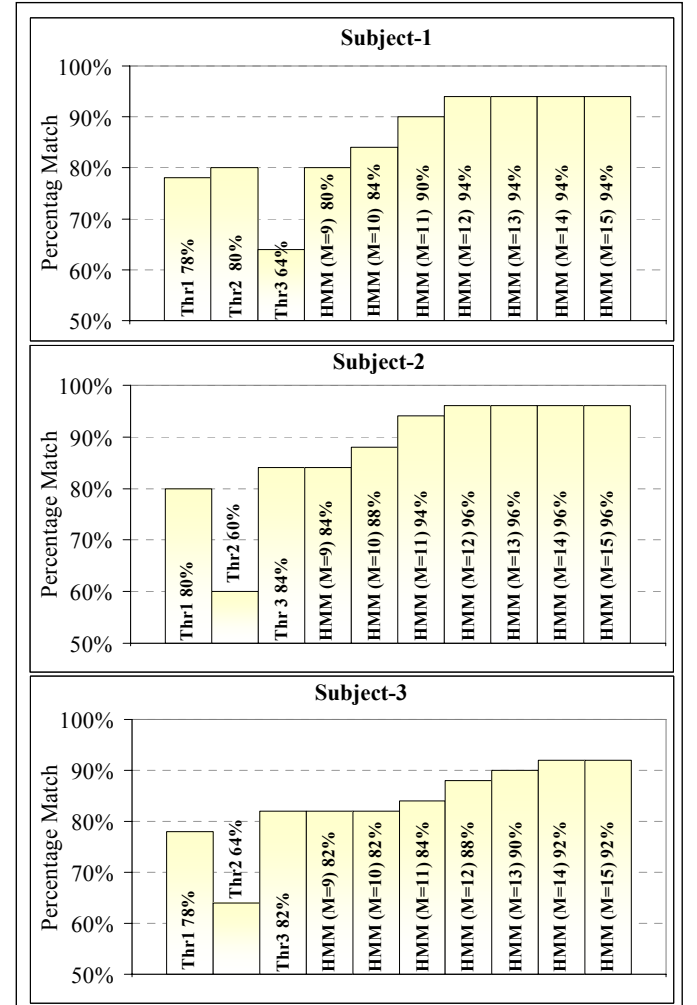


Fig. 8. Posture identification performance

C.2 Automatic Observation Calibration

For the results above, the observation probability matrix B has been constructed during an observation calibration phase before experimenting with each individual human subject. This calibration process (construction of matrix B based on observations) somewhat compensates for the inconsistencies in the observation values due to variations in clothing, personal posture specialties and other ambient differences. In fact this calibration process accounts a great deal for the consistently superior performance of HMM compared to the threshold based strategy, as presented in Figure 8.

In this section we implement a self-calibration process of the B matrix, so that the proposed posture identification mechanism can be more practically implemented without having to manually calibrate the B matrix for each individual subject.

We use the Baum-Welch iterative algorithm [20], for which the key idea is to start with initial B matrix, and then iteratively adjust it based on the stochastic difference between the identified (using HMM) posture state sequence and the expected sequence based on the notion of the state transition matrix A . Details of the Baum-Welch derivation and the algorithm are included in the Appendix.

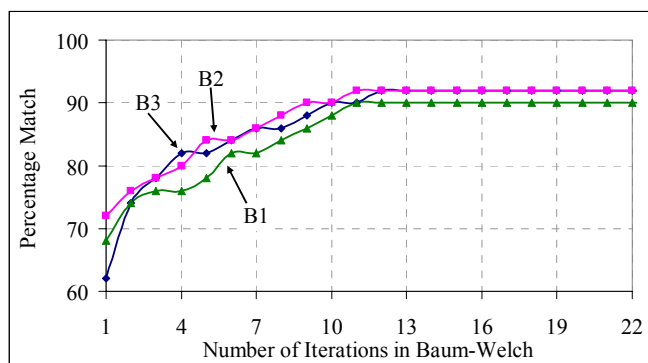


Fig. 9. Automatic self-calibration of the B matrix

Figure 9 demonstrates the performance of this self-calibration process in terms of the posture identification accuracy over multiple iterations. Here we used the observation sequence of human subject-2 of the last experiments, with observation granularity factor $M = 12$. Observe that with all three different initial B matrices, the identification accuracy gradually increases over time with Baum-Welch iterations. For all three cases, the posture identification process started delivering the best performance within 12 iterations. In a deployment sense, this means that after wearing the sensors, the subject should continue with his or her regular behavior for a while for allowing the network to self-calibrate the HMM B matrix. After that, the identified posture recording should start.

VI SUMMARY AND ONGOING WORK

We present an experimental framework for a wearable sensor network that can be used for networked human posture identification. A novel multi-modal sensing paradigm, coupled with Hidden Markov Model (HMM) based pattern identification techniques, has been used for detecting a wide range of human postures which are typically not differentiable using the traditional accelerometry based approaches. It was first demonstrated that although a naïve threshold based mechanism can be used for reasonable detection performance, the intrinsic errors and unpredictability of the on-body data collection process require a delicate dimensioning of the used threshold values for consistent posture identification performance across various human subjects. To avoid this, an HMM based detection process is applied with observation self-calibration using the Baum-Welch algorithm. It was

shown that the HMM method with our novel sensing modalities are able to consistently deliver significantly better detection performance than the threshold based mechanism in a more individual-independent manner. Ongoing work on this topic includes: 1) adjusting the HMM and processing mechanism to adapt for different baseline behaviors (the A matrix), 2) increasing the number of on-body sensors, and studying the impacts of network topologies on sensor energy consumption, and 3) extending the computation mode from out-of-body (used in this work) to on-body.

REFERENCES

- [1] S. Bao, Y. Zhang, and L. Shen, "Physiological Signal Based Entity Authentication for Body Area Sensor Networks and Mobile Healthcare Systems," 27th IEEE Conference on Engineering in Medicine and Biology, Shanghai, China, pp. 2455–2458, 2005.
- [2] B. Lo, S. Thiemjarus, R. King and G. Yang, "Body Sensor Network – A Wireless Sensor Platform for Pervasive Healthcare Monitoring," Proceedings of the 3rd International Conference on Pervasive Computing (PERVASIVE 2005), pp. 77–80, May 2005.
- [3] C. Otto, A. Milenkovic, C. Sanders, E. Jovanov, "System Architecture of a Wireless Body Area Sensor Network for Ubiquitous Health Monitoring," J. of Mobile Multimedia, Vol. 1, No. 4, pp. 307–326, 2006.
- [4] A. Milenkovic, C. Otto, E. Jovanov, "Wireless Sensor Networks for Personal Health Monitoring: Issues and an Implementation," to appear in Computer Communications (Special issue: Wireless Sensor Networks: Performance, Reliability, Security, and Beyond), Elsevier, 2006.
- [5] V. Senanarong, K. Harnphadungkit, N. Prayoonwiwat, N. Pongvarin, N. Sivasariyanonds, T. Printarakul, S. Udornpuntharak, J. Cummings, "A new measurement of activities of daily living for Thai elderly with dementia," International Psychogeriatrics 2003; 15(2):135–148.
- [6] M. Moh, B. Culpepper, T.-S. Moh, T. Hamada, and C.-F. Su, "On Data Gathering Protocols for In-body Biomedical Sensor Networks," Proceedings of 48th IEEE Globecom, St. Louis, MO, Nov 2005.
- [7] S.-W. Lee and K. Mase, "Activity and Location Recognition using Wearable Sensors," Pervasive Computing, vol. 1, no. 3, pp. 24–32, Jul.–Sep. 2002.
- [8] E. Jovanov, A. Milenković, C. Otto, P. De Groen, B. Johnson, S. Warren, and G. Taibi, "A WBAN System for Ambulatory Monitoring of Physical Activity and Health Status: Applications and Challenges," Proceedings IEEE Eng Med Biol Soc 4: 3810–3, 2005.
- [9] E. Jovanov, A. Milenkovic, C. Otto and P. C. de Groen, "A Wireless Body Area Network of Intelligent Motion Sensors for Computer Assisted Physical Rehabilitation," Journal NeuroEng. and Rehab., vol. 2, no. 11, p. 6, Mar. 2005.
- [10] <http://grants2.nih.gov/grants/guide/pa-files/PA-07-354.html>
- [11] K.Y. Chen, D.R. Bassett Jr, "The Technology of Accelerometry-based Activity Monitors: Current and Future," Med Sci Sports Exerc; 37:S490–500. doi: 10.1249/01.mss.0000185571.49104.82, 2005.
- [12] A. Ylisaukko-oja, E. Vildjiounaite, J. Mäntyjärvi, "Five-Point Acceleration Sensing Wireless Body Area Network - Design and Practical Experiences," 184–185, ISWC 2004.
- [13] E. Farella, A. Pieracci, A. Acquaviva, L. Benini, "A Wireless Body Area Sensor Network for Posture Detection" Computers and Communications, 2006. ISCC '06.
- [14] L. Bao and S. S. Intille, "Activity recognition from user-annotated acceleration data," In: Proceedings of the Second International Conference on Pervasive Computing, Vienna, Austria, 2004; 1–17.
- [15] A. Krause, D.P. Siewiorek, J. Farrington, "Unsupervised, dynamic identification of physiological and activity context in wearable computing," In: Proceedings of the Seventh IEEE International Symposium on Wearable Computers 2003; 88–

- 97.
- [16] M. Quwaider and S. Biswas, "Body Posture Identification using Hidden Markov Model with a Wearable Sensor Network," BodyNets, Tempe, Arizona, March 2008.
- [17] http://www.egr.msu.edu/~sbiswas/Research/wearable_proto.wmv
- [18] Crossbow Technology, Inc. <http://www.xbow.com>
- [19] B. Juang, "Maximum Likelihood Estimation for Mixture Multivariate Stochastic Observations of Markov Chains," AT&T Tech. I., vol. 64, no. 6, pp. 1235-1249, July-Aug. 1985.
- [20] L. Rabiner, "A Tutorial on Hidden Markov Models and Selected Applications in Speech Recognition," Proceedings of the IEEE, vol. 77, no. 2, pgs 257 - 285, Feb. 1989.
- [21] J. Allanach, H. Tu, S. Singh, K. Pattipati and P. Willet, "Detecting, Tracking and Counteracting Terrorist Networks via Hidden Markov Models," IEEE Aerospace, March 2004.
- [22] O. Brdiczka, and P. Reignier, "Automatic Detection of Interaction Groups," ICMI: 32-36, 2005.
- [23] V. Nair and J. Clark, "Automated Visual Surveillance using Hidden Markov Models," International Conference on Vision Interface, pp. 88 - 93, 2002.
- [24] L. Wang, M. Mehrabi, and E. Kannatey-Asibu, Jr. "Hidden Markov Model-based Tool Wear Monitoring in Turning," J. of Manufacturing Science and Engineering, Volume 124, Issue 3, pp. 651-658, August 2002.

APPENDIX: ITERATIVE HMM WITH AUTOMATIC OBSERVATION CALIBRATION

As proposed in [20][23], it is possible to calibrate the HMM parameters in λ such that the quantity $P(O|\lambda)$, representing the conditional probability of an observation sequence (of length T) is maximized. In our specific application of self-calibration as discussed in Section V.C, it is required to adjust the observation probability matrix B while keeping the other two parameters A and π in λ constant. The Baum-Welch algorithm [20] is used in our implementation to iteratively obtain an estimate of B that results in a λ which is guaranteed to locally maximize $P(O|\lambda)$.

As discussed in Section V.A, the element $b_{j,m}$ in the matrix B represents the probability that in posture state j , the elements c_m, x_m, r_m and k_m in the observation vector O are '1's' and the rest of the elements are all zero. The quantity $b_{j,m}$ can be

$$b_{j,m} \equiv \frac{\sum_{t=1}^T \gamma_t(j)}{\sum_{i=1}^T \gamma_t(j)} \quad (A.1)$$

where the denominator represents the probability that the system is always in state j with all possible observations. The numerator represents the probability that the system is in state j with a specific observation such that the elements v_m , where $v_m = \{c_m, x_m, r_m, k_m\}$ in the observation vector O are '1's' and the rest of the elements are all zero.

Using Equation A.1 as the iterative step for changing the B matrix, we have implemented the following algorithm for implementing self-calibration as explained in Section VI.A.2.

1. Collect observations $O = O_1 O_2 \dots O_T$
2. Initialize λ using a starting B matrix with constant A and π
3. Given observation sequence $O = O_1 O_2 \dots O_T$ and λ , compute: $\gamma_t(j), \forall 1 \leq t \leq T, 1 \leq j \leq N$
4. Compute new B matrix by updating the elements $b_{j,m}$ based on Equation A.1
5. Set new λ_{new} using the new B matrix
6. Compute a new quantity MAXLIKELIHOOD as:

$$MAX LIKELIHOOD = \max[P(O_1 \dots O_T | \lambda), P(O_1 \dots O_T | \lambda_{new})]$$

7. $\lambda = \lambda_{new}$

8. Go to step-3 and repeat till the quantity MAXLIKELIHOOD converges
- 9.

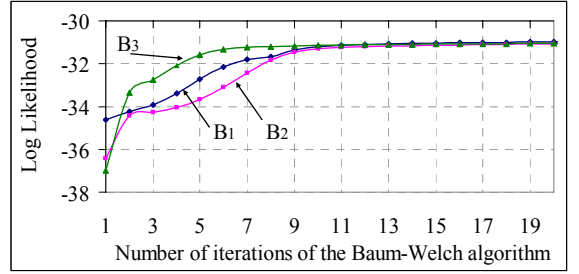


Figure 10: Performance of Baum-Welch iterative algorithm

The fact that the newly estimated B matrix in Step 4 is computed based on the actual observation sequence, ensures that the estimation would improve the quantity $P(O|\lambda)$. This accounts for the monotonically increasing nature of the MAXLIKELIHOOD, as evidenced in Figure 10, which demonstrates the convergence performance of the Baum-Welch algorithm in terms of the evolution of the log of the quantity MAXLIKELIHOOD. Observe that with all three different initial B matrices, the MAXLIKELIHOOD monotonically increases over the algorithm iterations, and converges approximately after 13 iterations, which is consistent with what has been reported in Figure 9.



Muhannad Quwaider received the BS degree in electrical and computer engineering from Jordan University of Science and Technology (JUST), Irbid, Jordan in 2000, and the MS degree in electrical and computer engineering from Michigan State University (MSU), East

Lansing, USA, in 2005. He is currently working toward the Ph.D. degree in Electrical and Computer Engineering at Michigan State University. His research interests include wireless sensor networks, mobile ad hoc networks, and body area network. He is a student member of the IEEE.



Subir Biswas is an Associate Professor and the Director of the Networked Embedded and Wireless Systems Laboratory at Michigan State University. Subir received his Ph.D. from the University of Cambridge and has held various research positions at the NEC

Research Institute, Princeton, AT&T Laboratories, Cambridge, and Tellium Optical Systems, NJ. He has published over 80 peer-reviewed articles in the area of network protocols, and is co-inventor of 3 U.S. patents. His current research interests include the broad area of wireless data networking, low-power network protocols, and application-specific sensor networks. He is a senior member of IEEE and a fellow of the Cambridge Philosophical Society.